

Comparative numerical study featuring magnetized nanofluids configured by elongating sheet with thermophoresis and Brownian motion

Srinivasa Rao Puchakayala^a, Shashidar Reddy Borra^b, Saritha Kallu^c, Shaira Formanova^d, M. Ijaz Khan^e, M. Waqas^{f,g,*}, Furqan Ahmad^h, Manish Guptaⁱ

^a Department of Mathematics, Malla Reddy Engineering College (Autonomous), Dhulapally, Hyderabad 500100, Telangana, India

^b Department of Mathematics, Sreenidhi Institute of Science and Technology, Ghatkesar, Hyderabad 501301, Telangana, India

^c Department of Humanities and Sciences (Mathematics), CVR College of Engineering, Ibrahimpatnam, Hyderabad 501510, Telangana, India

^d Department of Chemistry and Its Teaching Methods, Tashkent State Pedagogical University, Tashkent, Uzbekistan

^e Department of Mechanical Engineering, College of Engineering, Prince Mohammad Bin Fahd University, Al-Khobar, Saudi Arabia

^f NUTECH School of Applied Science and Humanities, National University of Technology, Islamabad 44000, Pakistan

^g Department of Computer Science and Mathematics, Lebanese American University, Beirut, Lebanon

^h Western Caspian University, Baku, Azerbaijan

ⁱ Division of Research and Development, Lovely Professional University, Phagwara, India

ARTICLE INFO

Keywords:

Hybrid nanofluid
Elongating sheet
Thermophoresis
Brownian motion
Hall current
Joule heating

ABSTRACT

This study investigates the heat and mass transfer characteristics of MHD rotating $\text{Fe}_3\text{O}_4\text{-Al}_2\text{O}_3/\text{H}_2\text{O}$ hybrid nanofluid flow over a three-dimensional stretching surface. Comparative analysis was conducted among the base fluid H_2O , $\text{Al}_2\text{O}_3\text{-H}_2\text{O}$ nanofluid, and $\text{Fe}_3\text{O}_4\text{-Al}_2\text{O}_3/\text{H}_2\text{O}$ hybrid nanofluid, focusing on velocity, temperature, and concentration distributions influenced by thermophoresis, Brownian motion, Hall current, temperature ratio, magnetic parameter, rotation, and thermal radiation. The governing nonlinear partial differential equations were transformed into ordinary differential equations using similarity adaptations and solved numerically with the BVP-5C method in MATLAB. Results indicate that increasing the thermophoresis and Brownian motion parameters elevates the temperature profile while affecting the concentration distribution differently. The hybrid nanofluid exhibited a higher temperature distribution compared to the nanofluid and base fluid, whereas the base fluid showed a greater concentration gradient.

1. Introduction

The shape of $\text{Fe}_3\text{O}_4\text{-Al}_2\text{O}_3$ hybrid nanoparticles significantly influences the behavior of fluid flow, particularly by affecting thermal conductivity, viscosity, and the distribution of heat within the fluid. Non-spherical nanoparticles, such as rods or platelets, typically have higher surface area-to-volume ratios, which can enhance thermal conductivity and heat transfer efficiency. However, these shapes may also increase the fluid's viscosity, potentially leading to greater flow resistance. The shape also impacts the Brownian motion and thermophoresis effects, which are crucial for the uniform distribution of temperature and concentration in the flow. These factors have practical implications for various applications, such as improving the efficiency of heat exchangers, enhancing cooling systems in electronics, and optimizing energy systems like solar collectors. By carefully selecting the shape of

hybrid nanoparticles, engineers can tailor fluid properties to meet specific industrial needs, leading to more effective and efficient thermal management solutions.

Analysing the dynamics of moving fluids, including liquids, gases and plasmas, holds significant relevance across various practical domains. Through this examination, researchers and engineers can enhance aircraft design for efficiency and safety, refine pipeline systems for optimal performance, advance capabilities in weather prediction, optimize marine vessel construction and gain insights into cardiovascular health by investigating blood circulation and foster innovation in technological development. Choi¹ pioneered the observation that the incorporation of nanoparticles, including graphene, silica, silver, gold, copper, alumina, ferrous ferric oxide, and carbon nanotubes, etc., with diameters ranging from 1 to 100 nm, into base liquids such as ethylene glycol, moistness, kerosene and engine oils can elevate their thermal conductivity. This augmentation subsequently enhances the fluid

* Corresponding author.

E-mail address: mw_qau88@yahoo.com (M. Waqas).

<https://doi.org/10.1016/j.padiff.2024.100915>

Received 26 May 2024; Received in revised form 3 September 2024; Accepted 7 September 2024

Available online 8 September 2024

2666-8181/© 2024 The Author(s). Published by Elsevier B.V. This is an open access article under the CC BY-NC-ND license (<http://creativecommons.org/licenses/by-nc-nd/4.0/>).

Nomenclature			
u, v, w	Velocity components along x, y and z-axes resp. (m s^{-1})	T_w	Temperature at the wall
μ_{hnf}	Viscosity of hybrid nanofluid ($\text{kg.m}^{-1}.\text{s}^{-1}$)	T_∞	Ambient temperature
σ_{hnf}	Electrical conductivity of hybrid nano fluid (S m^{-1})	C	Concentration of the fluid (mol/m^3)
ρ_{hnf}	Density of hybrid nano fluid (kg/m^3)	C_w	Concentration of the stretching sheet
β_{hnf}	Concentration diffusivity of hybrid nano fluid	C_∞	Concentration of the free stream
k_{hnf}	Thermal conductivity of hybrid nano fluid (W/m.K)	q_r	radiation flux
$(\rho C_p)_{hnf}$	Heat capacitance of hybrid nano fluid (J/Kg K)	ξ_1	constant rate of non-linear chemical reaction
k_{bf}	Thermal conductivity of $\text{Al}_2\text{O}_3/\text{H}_2\text{O}$ nanofluid (W/m.K)	σ^*	Stefan–Boltzman constant
μ_f	Dynamic viscosity of base fluid ($\text{kg.m}^{-1}.\text{s}^{-1}$)	α^*	Mean absorption co-efficient
ν_f	Kinematic viscosity of base fluid (m^2/s)	ω	angular velocity
ρ_f	Density of the base fluid (kg/m^3)	Pr	Prandtl number
β_f	Concentration diffusivity of fluid	η	Non-dimensional similarity variable
K_f	Thermal conductivity of base fluid (W/m.K)	ϕ_1, ϕ_2	Fe_3O_4 and Al_2O_3 nanoparticles volume fractions
$(\rho C_p)_f$	Heat capacitance of the base fluid (J/K)	Nt	Thermophoresis parameter
ρ_{s1}, ρ_{s2}	Density of Fe_3O_4 and Al_2O_3 nano particals (kg/m^3)	Nb	Brownian motion parameter
$(\rho C_p)_{s1}, (\rho C_p)_{s2}$	Heat capacitance of Fe_3O_4 and Al_2O_3 nanoparticles (J/Kg K)	m	Hall current
k_{s1}, k_{s2}	Thermal conductivity of Fe_3O_4 and Al_2O_3 nanoparticles	θ_w	Temperature ratio parameter
B_0	Magnetic field strength (A/m^{-1})	M	Magnetic field parameter
T	Temperature of the fluid (K)	Rd	Radiation parameter
		Sc	Schmidt number
		Rc	Chemical reaction parameter
		λ	Rotation parameter

system's overall heat transfer efficiency.²

Hybrid nanofluids, formed by dispersing a combination of two nanoparticles within the base fluid, exhibit enhanced thermal conductivity compared to both conventional nanofluids and their base fluids.³ These fluids exhibit a diverse array of applications, ranging from modern cooling methods in machinery and addressing heat surpluses in vehicles to innovative hybrid electric systems.⁴ They also contribute to advancements in energy storage technologies, gas detection capabilities, biomedical manufacturing and renewable energy generation. Moreover, hybrid nanofluids are instrumental in solar thermal innovations, transistor development and specialized refrigeration techniques.⁵ Extensive exploration by numerous researchers has delved into the movement of electrically conducting fluids within electromagnetic fields, known as magnetohydrodynamics (MHD).⁶ This area of study holds a prominent focus in modern metallurgy and metalworking operations, with applications extending across engineering domains such as MHD power generation, electrical furnaces, metal casting, nuclear reactor cooling and turbo machinery.⁷ Research into fluid flow over a stretched surface has garnered significant attention due to its indispensable utility across various modern industries and contemporary technologies. Its multitude of practical applications, particularly within chemical engineering and metallurgy, encompasses methodologies such as polymer extrusion, paper film delineation and exhibition, metallic plate cooling, searing rolling, synthetic fibre production, continued stretching of malleable flicks, and copper wire drawing.⁸ Numerous researchers have explored the diverse impacts on MHD nano and hybrid nanofluid flows across a stretching consistency.

Thermophoresis and Brownian movement play pivotal roles in shaping the properties of nano and hybrid nanofluids.⁹ Thermophoresis, a phenomenon where particles migrate from high temperature zones to lower temperature regions, plays a crucial role in particle aggregation, including the conveyance of electric charge carriers within semiconductors.¹⁰ On the additional arrow, Brownian movement pushes particles discontinued in a liquid to exhibit erratic movement, facilitating their migration from regions of high concentration to low concentration.¹¹ Together, these phenomena greatly enhance heat transfer properties, making them invaluable across various applications including Heat exchanger corrosion, electronic cooling, warmth exchange mechanisms, aerosol technology, solar accumulators, and silicon thin film deposition are some of the technologies that are being

developed.^{12,13} Iskandar et al.¹⁴ conducted a study on radiative MHD flow and thermal properties of Reiner-Philippoff non-Newtonian fluid considering the consequences of thermophoresis diffusion and Brownian movement. Arshad et al.¹⁵ delve into the dynamics of 3-D magnetohydrodynamic (MHD) nanoliquid gush over a dual lengthening consistency coupled with chemical response and thermo radiation, while also considering the existence of a glad magnetic specialization. Abdelmalek¹⁶ examines how Brownian movement and thermophoretic forces influence the outpour of electrically conducting Prandtl-Eyring nanofluid over a lengthened consistency. Jagadish et al.¹⁷ dissected the consequence of thermophoresis and Brownian movement on the behaviour of thermal and chemically responding Casson nanoliquid stream over a linearly lengthening sheet. Meanwhile, Mehta and Kataria¹⁸ focus on analysing the consequences of Brownian movement and thermophoresis on MHD flow of a viscoelastic liquid over a lengthening sheet, considering thermal radiation and chemical responses.

In 1879, American physicist Hall introduced the concept of the Hall current,¹⁹ which occurs when a high-intensity magnetic field is applied to a low-density ionic liquid, transforming typical conduction perpendicular to the magnetic field into the rotational movement of collisions between atomic particles and ions along the magnetic field lines, which results in the induction of a current that is perpendicular to both the electric field and the magnetic field's lines of influence.²⁰ To accommodate an alternative interpretation of Ohm's law is the Hall current becomes essential.²¹ Researchers have extensively investigated the flow of hybrid nanofluids with Hall current, as it finds applications in Hall accelerators, sensors, electric inverters, transformers, turbines, pumps, magnetometers, refrigerator coils, planetary fluid dynamics, power generators and more.^{22,23} Alzahrani²⁴ explored how Hall current and the presence of motile microorganisms influence the flow of nanofluid induced by a rotating disk, while accounting for various slip conditions and the effects of thermal radiation. While a Casson nanofluid was moving across an exponentially stretched surface, Suresh Kumar and colleagues²⁵ investigated the flow properties, heat transfer, and mass transfer characteristics of the fluid. A number of different aspects were taken into consideration in their research, including activation energy, Hall current, thermal radiation, Brownian motion, heat source/sink, and thermophoresis.

Incorporating the Joule heating effect in MHD flow studies is significant because it directly impacts the thermal energy within the fluid,

leading to enhanced heat transfer performance. Joule heating, caused by the interaction of an electric current with the magnetic field in a conducting fluid, generates additional heat, which can influence the temperature distribution and overall energy balance within the flow. This effect is particularly important in applications where precise thermal management is crucial, such as in cooling systems, nuclear reactors, and aerospace technologies. By accounting for Joule heating, the analysis becomes more accurate, allowing for better optimization of the fluid's thermal properties and the design of systems that utilize MHD flows for enhanced performance. This inclusion can lead to improved efficiency and reliability in processes where magnetic fields are used to control fluid flow and heat transfer. Joule pioneered the concept of Joule heating in 1840,²⁶ where heat is produced as a result of the flow of electric current through a resistive substance, a phenomenon also referred to as resistive or Ohmic heating.²⁷ Researchers have extensively explored Joule heating's implications for heat transmission applications. This phenomenon finds widespread use in electric heaters/stoves, industrial processes, cooking appliances resistance ovens and various heating elements, converting electrical energy into heat. Its significance extends to electrical systems, where it prevents component overheating in high-current environments.^{28,29} Ramzan et al.³⁰ possessed the implications of Hall current, Joule heating and variable thickness on the dual-direction flow above an extended surface. Madiha et al.³¹ investigated the consequences of Joule heating and dissipation on the flow of a magnetohydrodynamic ternary-hybrid nanofluid over an elongated surface embedded in a porous medium with Darcy Forchheimer characteristics. Using finite element techniques, Ullah et al.³² investigated the effects of Joule heating and thermal radiation on the boundary layer flow of an Oldroyd-B nanofluid with magnetohydrodynamics across a porous stretching surface. They found that these two factors had a significant impact on the flow through the boundary layer. Elsaid et al.³³ delved into the examination of the effects of joule heating, magnetic field, Hall current, nonlinear thermal radiation and rotational parameter over-stretched plate immersed in a rotating hybrid nanofluid comprised of Fe_3O_4 and Al_2O_3 .

Hybrid nanofluids typically demonstrate superior thermal performance compared to conventional nanofluids, owing to the collaborative influence of diverse nanoparticle compositions. The amalgamation of these nanoparticles has shown to enhance stability, thermal conductivity and heat transfer efficacy. In the present scenario, researchers are interested in exploring the impact of non-dimensional parameters on hybrid nanofluid and nanofluid flows by conducting comparative analyses. In,³⁴ Ramzan et al. state that hybrid nanofluids exhibit superior thermal characteristics and stability compared to their single-component counterparts. Moreover, these hybrid nanofluids surpass both single-particle nanofluids and their respective base fluids in terms of cooling efficiency. In,³⁵ Alharbi et al. meticulously examined the comparative analysis between MHD SWCNTs-Ethylene glycol nanofluid and DWCNTs-SWCNTs-Ethylene glycol hybrid nanofluid on a bi-directional stretching surface, incorporating Cattaneo-Christov heat flux. Similarly, in,³⁶ the same researchers explored the impacts of Hall current and ion slip considering zinc oxide and gold nanoparticles dispersed in both kerosene oil and water to form distinct hybrid nanofluids. Their findings highlight the superior heat transfer rates of the ZnO-Au/ H_2O combination compared to ZnO-Au/kerosene oil. Lu et al.³⁷ conducted a comparative investigation on Ag-water nanofluid and Ag-CuO/water hybrid nanofluid with Darcy-Forchheimer flow over a curved surface. Employing a stagnation point flow model, Gul et al.³⁸ assessed the energy transient across the nanofluid through a comparative analysis. Recently, Alzahrani and Khan,⁴⁶ Mishra et al.,⁴⁷ Raja et al.,⁴⁸ Khan et al.⁴⁹ and Xiang et al.⁵⁰ operated different fluid flow subject to complex flow geometries in the presence multiple boundary constraints.

The novelty of this study lies in its comprehensive comparative analysis of base fluids, nanofluids, and hybrid nanofluids under the simultaneous influence of thermophoresis, Brownian motion, and magnetohydrodynamics (MHD) within a three-dimensional stretching

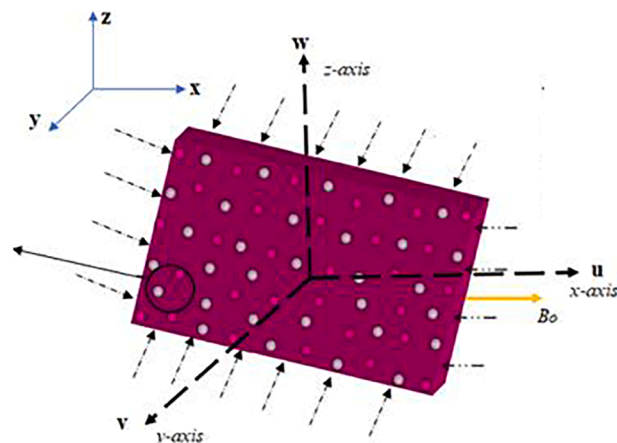


Fig. 1. Geometry of the flow and coordinate system.

surface configuration. Unlike previous research that has predominantly focused on single-component nanofluids or simpler flow scenarios, this study expands the understanding of fluid dynamics and heat transfer by exploring more complex geometries and interactions. Additionally, the application of the BVP-5C method in MATLAB, coupled with a shooting approach, offers a more accurate and efficient solution to the nonlinear governing equations, providing new insights into the behavior of hybrid nanofluids like $Fe_3O_4-Al_2O_3/H_2O$. These contributions collectively enhance the understanding of how hybrid nanofluids can be optimized for industrial applications, filling a significant gap in the existing literature.

2. Mathematical formulation of the problem

We consider heat and mass transfer characteristics of a magnetohydrodynamic (MHD) rotating flow of a hybrid nanofluid composed of Fe_3O_4 and Al_2O_3 nanoparticles suspended in water over a three-dimensional stretching surface. The governing equations, which include the continuity, momentum, energy, and concentration equations, are derived under the influence of physical phenomena such as thermophoresis, Brownian motion, Hall current, and thermal radiation. These nonlinear partial differential equations are transformed into a set of ordinary differential equations using similarity transformations. The boundary conditions at the stretching surface and at infinity are applied to solve these equations. The study employs the BVP5C numerical method to obtain the solutions, which are then used to calculate critical physical quantities such as the skin friction coefficients, local Nusselt number, and Sherwood number, providing a comprehensive understanding of the fluid dynamics and heat transfer behavior in the system. The physical configuration of the problem showed in Fig. 1.

Under the stated assumptions, three dimensional non-linear technique of PDEs that encloses continuity, rate, dynamism and conservation can be expressed as follows (Elsaid et al.³³):

$$\frac{\partial u}{\partial x} + \frac{\partial v}{\partial y} + \frac{\partial w}{\partial z} = 0 \quad (1)$$

$$\rho_{hnf} \left(u \frac{\partial u}{\partial x} + v \frac{\partial u}{\partial y} + w \frac{\partial u}{\partial z} - 2\omega v \right) = \mu_{hnf} \left(\frac{\partial^2 u}{\partial z^2} \right) - \frac{\sigma_{hnf} B_0^2}{(1+m^2)} (u - mv) \quad (2)$$

$$\rho_{hnf} \left(u \frac{\partial v}{\partial x} + v \frac{\partial v}{\partial y} + w \frac{\partial v}{\partial z} + 2\omega u \right) = \mu_{hnf} \left(\frac{\partial^2 v}{\partial z^2} \right) - \frac{\sigma_{hnf} B_0^2}{(1+m^2)} (v + mu) \quad (3)$$

Table 1

Thermo material possessions of Al₂O₃/H₂O nanofluid and Fe₃O₄ - Al₂O₃/H₂O hybrid nanofluid.³⁹⁻⁴²

Properties	Al ₂ O ₃ - H ₂ O nanofluid
Viscosity (μ)	$\mu_{nf} = \frac{\mu_f}{(1 - \phi_2)^{2.5}}$
Density (ρ)	$\rho_{nf} = (1 - \phi_2)\rho_f + \phi_2\rho_{s_2}$
Heat capacity (ρC _p)	$(\rho C_p)_{nf} = (1 - \phi_2)(\rho C_p)_f + \phi_2(\rho C_p)_{s_2}$
Thermal conductivity (k)	$\frac{k_{nf}}{k_f} = \frac{k_{s_2} + 2k_f - 2\phi_2(k_f - k_{s_2})}{k_{s_2} + 2k_f + \phi_2(k_f - k_{s_2})}$
Electrical conductivity (σ)	$\frac{\sigma_{nf}}{\sigma_f} = \frac{\sigma_{s_2} + 2\sigma_f - 2\phi_2(\sigma_f - \sigma_{s_2})}{\sigma_{s_2} + 2\sigma_f + \phi_2(\sigma_f - \sigma_{s_2})}$
Properties	Fe ₃ O ₄ - Al ₂ O ₃ /H ₂ O hybrid nanofluid
Viscosity (μ)	$\mu_{hnf} = \frac{\mu_f}{(1 - \phi_1)^{2.5}(1 - \phi_2)^{2.5}}$
Density (ρ)	$\rho_{hnf} = (1 - \phi_2)\{(1 - \phi_1)\rho_f + \phi_1\rho_{s_1}\} + \phi_2\rho_{s_2}$
Concentration diffusivity (β)	$\beta_{hnf} = (1 - \phi_1)(1 - \phi_2)\beta_f$
Heat capacity (ρC _p)	$(\rho C_p)_{hnf} = (1 - \phi_2)\{(1 - \phi_1)(\rho C_p)_f + \phi_1(\rho C_p)_{s_1}\} + \phi_2(\rho C_p)_{s_2}$
Thermal conductivity (k)	$\frac{k_{hnf}}{k_{bf}} = \frac{k_{s_2} + 2k_{bf} - 2\phi_2(k_{bf} - k_{s_2})}{k_{s_2} + 2k_{bf} + \phi_2(k_{bf} - k_{s_2})}$, where $\frac{k_{bf}}{k_f} = \frac{k_{s_1} + 2k_f - 2\phi_1(k_f - k_{s_1})}{k_{s_1} + 2k_f + \phi_1(k_f - k_{s_1})}$
Electrical conductivity (σ)	$\frac{\sigma_{hnf}}{\sigma_{bf}} = \frac{\sigma_{s_2} + 2\sigma_{bf} - 2\phi_2(\sigma_{bf} - \sigma_{s_2})}{\sigma_{s_2} + 2\sigma_{bf} + \phi_2(\sigma_{bf} - \sigma_{s_2})}$, where $\frac{\sigma_{bf}}{\sigma_f} = \frac{\sigma_{s_1} + 2\sigma_f - 2\phi_1(\sigma_f - \sigma_{s_1})}{\sigma_{s_1} + 2\sigma_f + \phi_1(\sigma_f - \sigma_{s_1})}$

$$(\rho C_p)_{hnf} \left(u \frac{\partial T}{\partial x} + v \frac{\partial T}{\partial y} + w \frac{\partial T}{\partial z} \right) = k_{hnf} \left(\frac{\partial^2 T}{\partial z^2} \right) + \frac{\partial^2 T^4}{\partial z^2} \left(\frac{4\sigma^*}{3\alpha^*} \right) + \sigma_{hnf} B_0^2 (u^2 + v^2) + \tau \left[\frac{D_T}{T_\infty} \left(\frac{\partial T}{\partial z} \right)^2 + D_B \left(\frac{\partial C}{\partial z} \right) \left(\frac{\partial T}{\partial z} \right) \right] \quad (4)$$

$$u \frac{\partial C}{\partial x} + v \frac{\partial C}{\partial y} + w \frac{\partial C}{\partial z} = \beta_{hnf} \left(\frac{\partial^2 C}{\partial z^2} \right) - K_r^2 (C - C_\infty) \left(\frac{T}{T_\infty} \right)^m \exp \left(\frac{-E_a}{K^* T} \right) \quad (5)$$

With the following boundary conditions (Elsaid et al.³³)

$$u = u_w, v = 0, w = 0, T = T_w, C = C_w \text{ at } z = 0$$

$$u \rightarrow 0, v \rightarrow 0, T \rightarrow T_\infty, C \rightarrow C_\infty \text{ as } z \rightarrow \infty \quad (6)$$

In accordance with the Roseland approximation, the radiation flux includes the following by,⁴³

$$q_r = \frac{-4\sigma^*}{3\alpha^*} \frac{\partial T^4}{\partial z} \quad (7)$$

The similitude mutations are characterized as (Elsaid et al.³³)

$$u = bxf'(\eta), v = bxg(\eta), w = -\sqrt{b\nu_f}f(\eta), \eta = \sqrt{\frac{b}{\nu_f}}z, T = T_\infty + (T_w - T_\infty)\theta(\eta), C = C_\infty + (C_w - C_\infty)\phi(\eta). \quad (8)$$

Following are the non-dimensional parameters

Table 2
Thermo physical properties of Fe₃O₄, Al₂O₃ and H₂O.³⁹

Properties	Fe ₃ O ₄	Al ₂ O ₃	H ₂ O
k (W/mK)	9.7	40	0.613
C _p (J/kgK)	670	765	4179
ρ (kg/m ³)	5180	3970	997.1
σ (Ω/m)	25 × 10 ³	35 × 10 ⁶	5 × 10 ⁻²
Pr			6.2

$$\lambda = \frac{\omega}{b}, \nu_f = \frac{\mu_f}{\rho_f}, M = \frac{\sigma_f B_0^2}{b\rho_f}, Pr = \frac{\nu_f(\rho C_p)_f}{k_f}, Ec = \frac{u_w^2 \rho_f}{(\rho C_p)_f(T_w - T_\infty)}, \theta_w = \frac{T_w}{T_\infty}, u_w = bx, Sc = \frac{\nu_f}{D_B}, Rc = \frac{\xi_1(C - C_\infty)^{n-1}}{b}, Nt = \frac{D_T \tau (T_w - T_\infty)}{\nu_f T_\infty}, Nb = \frac{D_B \tau (C_w - C_\infty)}{\nu_f} \quad (9)$$

Exploiting the similitude mutations (8) and the non-dimensional specifications (9), Eq. (1) is inherently fulfilled, while Eqs. (2)–(5) are transformed into the subsequent equations:

$$\left(\frac{l_4}{l_1}\right) f''' - f'^2 + ff'' + 2\lambda g - \left(\frac{l_5}{l_1}\right) \frac{M}{(1+m^2)} (f' - mg) = 0 \quad (10)$$

$$\left(\frac{l_4}{l_1}\right) g'' + fg' - f'g - 2\lambda f' - \left(\frac{l_5}{l_1}\right) \frac{M}{(1+m^2)} (g + mf) = 0 \quad (11)$$

$$\left(1 + \left(\frac{Rd}{l_3}\right) [1 + (\theta_w - 1)\theta]^3\right) \theta'' + Pr \left(\frac{l_2}{l_3}\right) f\theta' + \left(\frac{3Rd}{l_3}\right) [1 + (\theta_w - 1)\theta]^2 (\theta_w - 1)\theta'^2 + \left(\frac{l_5}{l_3}\right) M Ec Pr (f'^2 + g^2) + \frac{Pr}{l_3(\rho C_p)_f} (Nt \theta'^2 + Nb\phi'\theta) = 0 \quad (12)$$

$$\theta'' + \frac{Sc}{(1 - \phi_1)(1 - \phi_2)} (f + g)\theta' - K_E (1 + \theta)^m \phi \exp \left(\frac{-E}{1 + \theta} \right) = 0 \quad (13)$$

Where, $l_1 = \frac{\rho_{hnf}}{\rho_f}, l_2 = \frac{(\rho C_p)_{hnf}}{(\rho C_p)_f}, l_3 = \frac{k_{hnf}}{k_f}, l_4 = \frac{\mu_{hnf}}{\mu_f}, l_5 = \frac{\sigma_{hnf}}{\sigma_f}, l_6 = \frac{\beta_{hnf}}{\beta_f}$

Besides the thermo material possessions of Al₂O₃/H₂O nanofluid and Fe₃O₄ - Al₂O₃/H₂O hybrid nanofluid are defined via Table 1. The transformed boundary conditions are

$$f(\eta) = 0, f'(\eta) = 1, g(\eta) = 0, \theta(\eta) = 1, \phi(\eta) = 1 \text{ at } \eta = 0$$

$$f(\eta) \rightarrow 0, g(\eta) \rightarrow 0, \theta(\eta) \rightarrow 0, \phi(\eta) \rightarrow 0 \text{ as } \eta \rightarrow \infty \quad (14)$$

3. Mathematical expressions for sherwood number, nusselt number, and skin friction

These expressions account for the impact of the relevant non-dimensional parameters such as the Reynolds number, viscosity ratio, thermal conductivity ratio, and radiation effects on the hybrid nanofluid flow over a stretching surface.

The skin friction coefficient along the x-axis (C_{fx}) and y-axis (C_{fy}) are given by:

$$ReC_{fx} = \frac{\mu_{hnf}}{\mu_f} f''(0) \quad (15)$$

$$ReC_{fy} = \frac{\mu_{hnf}}{\mu_f} g'(0) \quad (16)$$

The local Nusselt number (Nux), which represents the dimensionless temperature gradient at the surface, is given by:

$$NuxRe^{-1/2} = -\left(\frac{k_{hnf}}{k_f} + Rd.\theta_w^3\right) \theta'(0) \quad (17)$$

The Sherwood number Shx, which represents the dimensionless concentration gradient at the surface, is given by:

$$ShxRe^{-1/2} = -\frac{k_{hnf}}{k_f} \phi'(0) \quad (18)$$

where: f'(0) and g'(0) are the derivatives of the velocity profiles at the

Table 3
Comparison of $f''(0)$ and $g'(0)$ with previous studies.

λ	Mustafa et al. ⁴⁴		Abdel-Wahed ⁴⁵		Elsaid et al. ³³		Current Study	
	$f''(0)$	$g'(0)$	$f''(0)$	$g'(0)$	$f''(0)$	$g'(0)$	$f''(0)$	$g'(0)$
0.50	-1.13838	-0.51276	-1.13837	-0.51276	-1.13838	-0.51276	-1.138887	-0.513234
1.00	-1.32503	-0.83709	-1.32503	-0.83710	-1.32503	-0.83710	-1.324959	-0.837051
2.00	-1.65235	-1.28726	-1.65235	-1.28726	-1.65235	-1.28726	-1.652354	-1.287258

Table 4
Comparison of Nusselt number with previous studies.

Rd	Rd and θ_w	Mustafa et al. ⁴⁴	Elsaid et al. ³³	Current Study
0	1	1.85767	1.85678	1.792838
1	1	2.23985	2.23980	2.199043
1	1.2	2.30458	2.30660	2.270439
1	1.5	2.60934	2.60093	2.587576

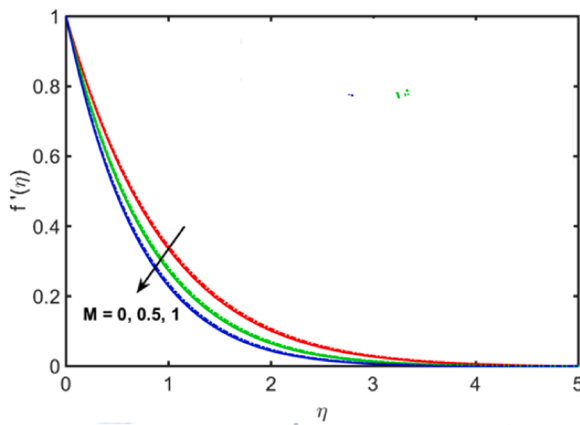


Fig. 2. Effect of magnetic parameter (M) on $f(\eta)$.

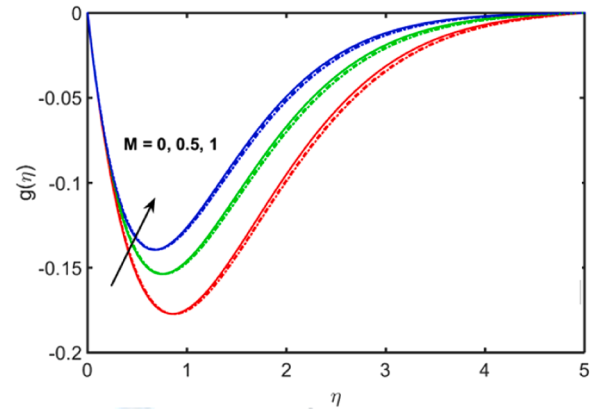


Fig. 3. Effect of magnetic parameter (M) on $g(\eta)$.

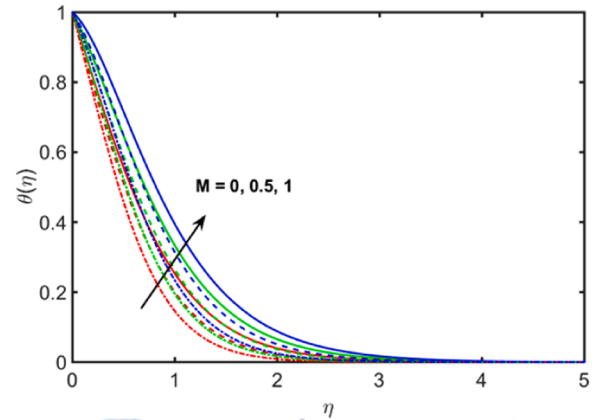


Fig. 4. Effect of magnetic parameter (M) on $\theta(\eta)$.

wall, μ_{hnf} , μ_f are the dynamic viscosities of the hybrid nanofluid and base fluid, respectively, Re is the Reynolds number, $\theta'(0)$ is the derivative of the temperature profile at the wall, k_{hnf} and k_f are the thermal conductivities of the hybrid nanofluid and base fluid, respectively, Rd is the radiation parameter, θ_w is the temperature ratio parameter, $\varphi'(0)$ is the derivative of the concentration profile at the wall. The thermo-physical characteristics of nanoparticles and base fluid is displayed in (Table 2).

Assessing the validity of the numerical investigation involves a comparison of the skin friction coefficient along the x-axis $f''(0)$ and y-axis $g'(0)$ across multiple rotation parameter (λ) values with those reported in previous literature. Table 3 demonstrate the validation process of the current research in contrast to earlier studies conducted by Mustafa et al. ,⁴⁴ Abdel-Wahed⁴⁵ and Elsaid et al.³³ across various λ values. The latest findings indicate a strong agreement with the existing results, particularly under specific parameters when $M = m = \phi_1 = \phi_2 = Rd = \theta_w = Ec = Sc = Rc = Nt = 0$ and $Nb = 0.0001$.

Table 4 exhibit the validation process of the Nusselt number in the current investigation, comparing it with prior research conducted by Mustafa et al.⁴⁴ and Elsaid et al. .³³ The comparison is made across two scenarios: the first with $Rd = 0$ and $\theta_w = 1$, and the second with $Rd = 1$ and varying θ_w values of 1, 1.1 and 1.5. In accordance with Karl Pearson’s approach, the coefficient of correlation (r) reveals a perfect positive correlation, close to 1, between current and past outcomes. This indicates a strong association between present and prior Nusselt number values provided in,^{33,44} especially under specific conditions, namely when $\phi_1 = 0.1, M = 1, \lambda = 0.5, \phi_2 = m = Ec = Sc = Rc = Nt = 0, Nb = 0.0001$.

4. Results and discussion

This work examine the heat and mass transfer characteristics of MHD rotating hybrid nanofluid $Fe_3O_4 - Al_2O_3/H_2O$ flow over three-dimensional linear stretching surface. A comparison has been showed among base fluid $H_2O, Al_2O_3 - H_2O$ nanofluid, $Fe_3O_4 - Al_2O_3/H_2O$ hybrid nanofluid on velocity, temperature and concentration fields under the influence of governing parameters, namely, thermophoresis, Brownian motion, hall current, temperature ratio parameter, magnetic parameter, rotation parameter, thermal radiation, Eckert number, Schmidt number, chemical reaction parameter, involving in the problem. During the computation of skin friction coefficients along the x ($\sqrt{Re} C_{fx}$) and y ($\sqrt{Re} C_{fy}$) axes, as well as the determination of local Nusselt ($Re^{-\frac{1}{2}} Nu$) and Sherwood numbers ($Re^{-\frac{1}{2}} Sh$), a consistent set of parameters was employed: $\phi_1 = 0.1, \phi_2 = 0.05, \lambda = 1, M = 0.5, Rd = 0.5, \theta_w = 1.2, Ec = 0.5, Sc = 0.22, Rc = 0.5, Nt = Nb = 0.5, m = 2$. Notably, alterations to one parameter were made while holding all others constant throughout the analysis.

Figs. 2–4 illustrate the magnetic parameter (M) effects on the flow

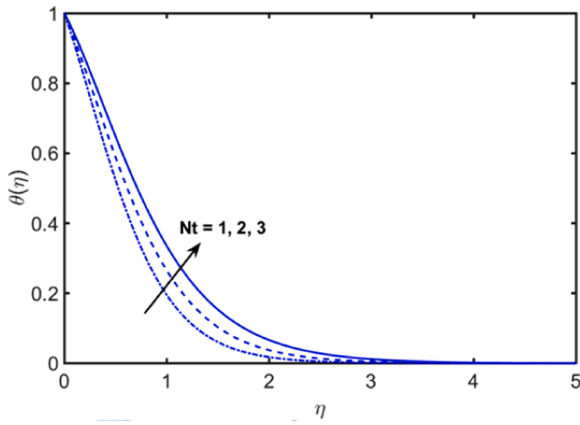


Fig. 5. Effect of thermophoresis parameter (Nt) on $\theta(\eta)$.

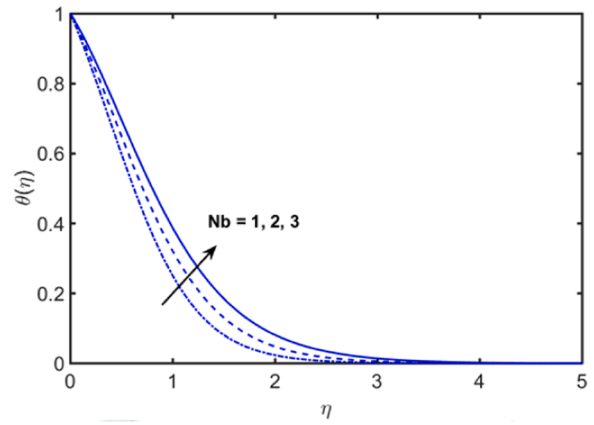


Fig. 7. Effect of Brownian motion (Nb) on $\theta(\eta)$.

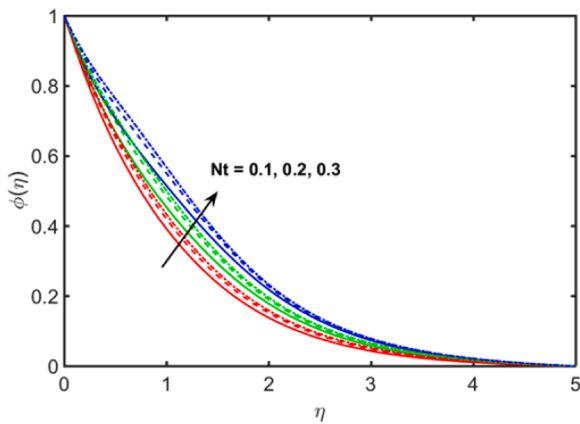


Fig. 6. Effect of thermophoresis parameter (Nt) on $\phi(\eta)$.

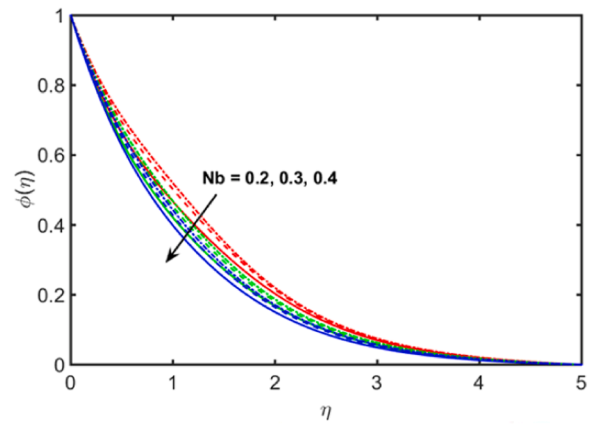


Fig. 8. Effect of Brownian motion (Nb) on $\phi(\eta)$.

characteristics of hybrid nanofluid, nanofluid and base fluid. The plots depict velocity profiles along the x- and y-axes, represented by $f(\eta)$ and $g(\eta)$, as well as the temperature profile $\theta(\eta)$. As M increases, $f(\eta)$ shows a decrease, while both $g(\eta)$ and $\theta(\eta)$ exhibit an increase. As the magnetic field strength increases, the external force acting perpendicularly on the flowing fluid becomes more pronounced. Consequently, the Lorentz force, originating from the magnetic field, hinders and disrupts the movement of fluid particles. This effect results in a decrease in fluid velocity along the x-axis and an increase in velocity along the y-axis. Additionally, this force intensifies interactions within the magnetic domain, leading to an augmentation in both boundary layer thickness and reinforcement of the temperature profile. The hybrid nanofluid exhibits a higher temperature profile compared to both the nanofluid and the base fluid, while the velocity profile of water surpasses that of both the nano and hybrid nanofluid.

Figs. 5 and 6 depict how thermophoresis parameter (Nt) influences the temperature ($\theta(\eta)$) and concentration ($\phi(\eta)$) profiles of the three fluids, namely, $Fe_3O_4 - Al_2O_3/H_2O$ hybrid nanofluid, $Al_2O_3 - H_2O$ nanofluid and the base fluid H_2O . The observation from these figures reveals that an increase in Nt results in a corresponding increase in both $\theta(\eta)$ and $\phi(\eta)$. Physically, elevating Nt results in an augmentation of the thermophoresis force, leading to a nanoparticle movement from the heated region to the cooler one. This process results in an elevation of temperature and an increase in the thickness of the boundary layer, causing a simultaneous rise in both profiles. Moreover, it has been noted that the temperature profile of the hybrid nanofluid is elevated in comparison to both the nanofluid and the base fluid, water. Conversely, the concentration profile demonstrates a completely contrasting trend.

The distributions of $\theta(\eta)$ and $\phi(\eta)$ for hybrid nanofluid, nanofluid and

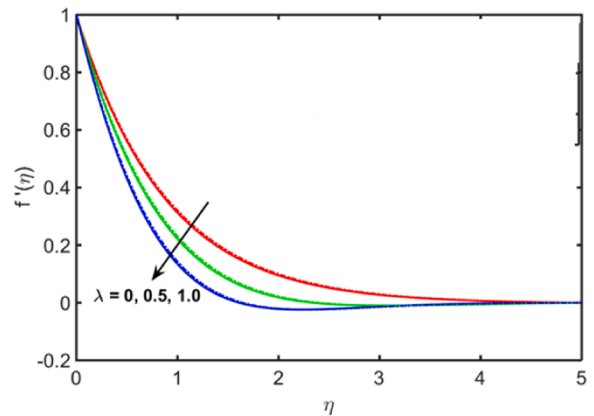


Fig. 9. Effect of rotation parameter (λ) on $f(\eta)$.

base fluid are notably influenced by Brownian motion (Nb), as illustrated in Figs. 7 and 8. An escalation in Nb values corresponds to an elevation in $\theta(\eta)$ and a reduction in $\phi(\eta)$. Physically, as Nb intensifies, the erratic movement of nanoparticles escalates, fostering heightened interactions among them. This transfer of kinetic significance through collisions from the microparticles to the liquid results in an augmented thermal boundary layer consistency, consequently elevating the temperature profile. Additionally, increased values hinder the dispersion of nanoparticles from the designated region, leading to a persistent decline in concentration distribution. Similarly, it is marked that the

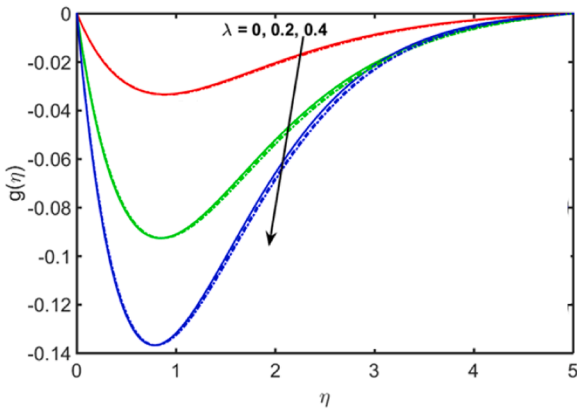


Fig. 10. Effect of rotation parameter (λ) on $g(\eta)$.

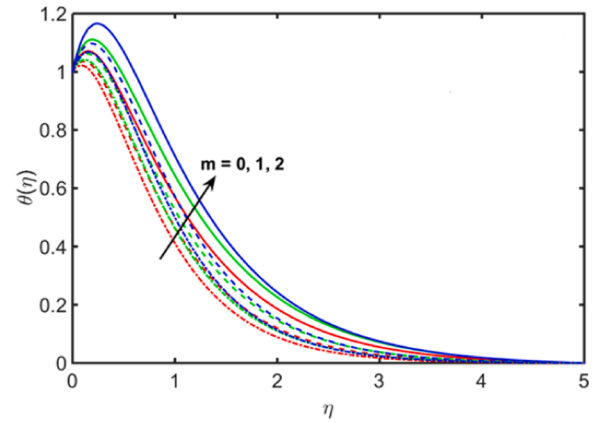


Fig. 13. Effect of hall current m on $\theta(\eta)$.

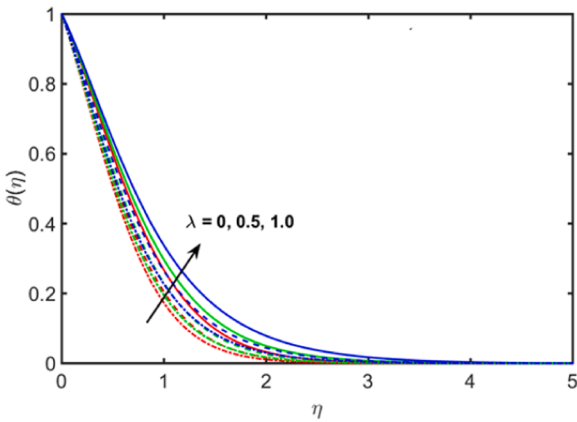


Fig. 11. Effect of rotation parameter (λ) on $\theta(\eta)$.

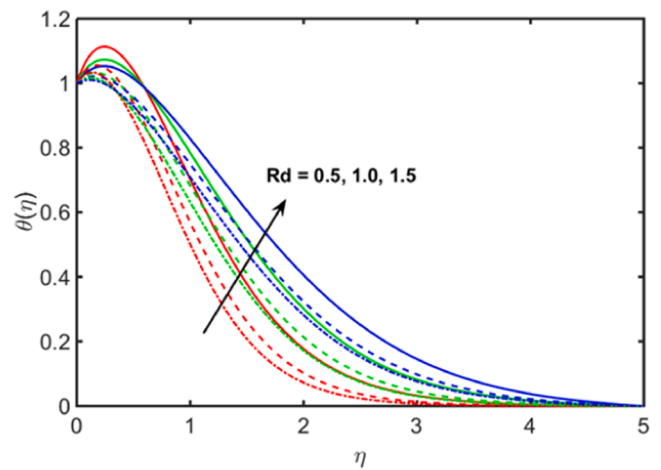


Fig. 14. Effect of radiation parameter Rd on $\theta(\eta)$.

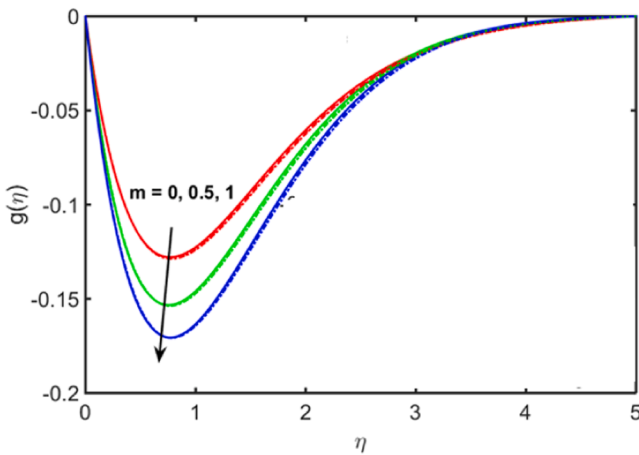


Fig. 12. Effect of Hall current m on $g(\eta)$.

temperature profile of the hybrid nanofluid is more increased than that of both the nanofluid and the base fluid. In contrast, the concentration profile of the base fluid surpasses that of both the nanofluid and the hybrid nanofluid.

The consequence of the rotation factor (λ) on the distributions of $f(\eta)$, $g(\eta)$ and $\theta(\eta)$ is illustrated in Figs. 9–11. Essentially, the rotation factor signifies the ratio of rotation rate to stretching rate. Higher values of λ denote a diminished stretching rate relative to the rotation rate, causing a reduction in the velocity profile along both the x- and y-axes. With the escalation of the rotation parameter, there is a concurrent rise

in the kinetic energy of the fluid, leading to an increase in temperature. It is obeyed that the momentum profile along the y-axis and temperature distribution are higher for the hybrid nanofluid, followed by the nanofluid and the underneath fluid. Conversely, an opposing tendency is noted for the momentum profile along the x-axis.

The significance of the Hall parameter, represented as m , becomes evident in the context of hybrid nanofluid flow, notably influencing $g(\eta)$ and $\theta(\eta)$ as depicted in Figs. 12 and 13. An increase in the parameter m

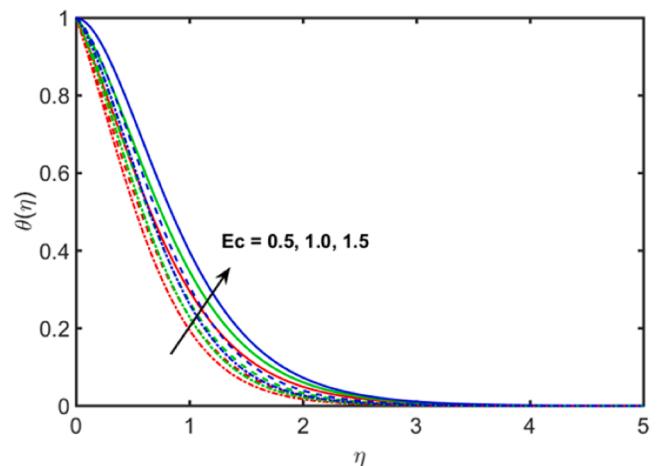


Fig. 15. Effect of Eckert number (Ec) on $\theta(\eta)$.

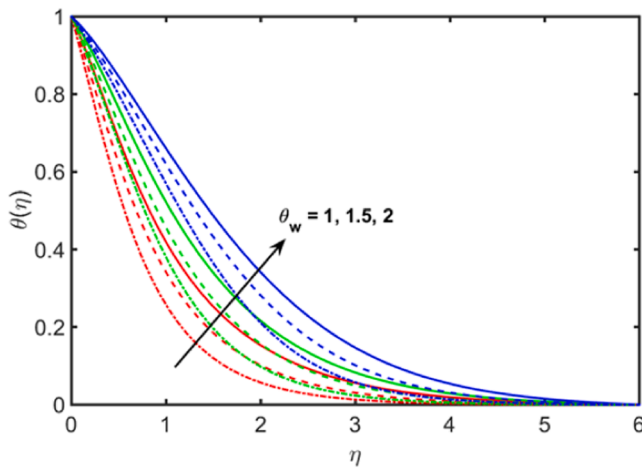


Fig. 16. Effect of Temperature ratio parameter (θ_w) on $\theta(\eta)$.

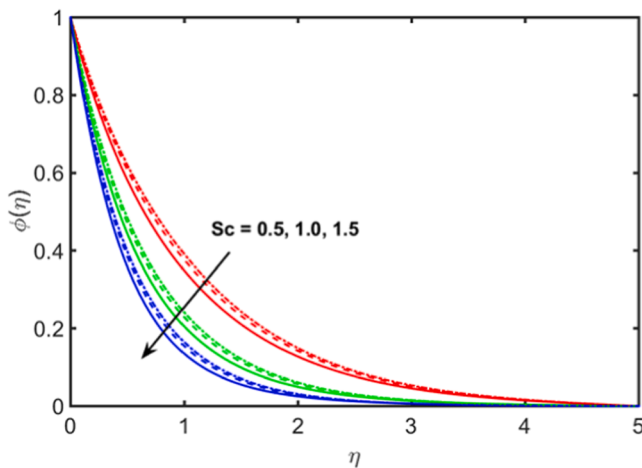


Fig. 17. Effect of Schmidt number (Sc) on $\phi(\eta)$.

correlates with a decrease in $g(\eta)$ and an increase in $\theta(\eta)$. This behaviour can be ascribed to the diminishing value of m as m rises. The decline in this value weakens the magnetic force, resulting in a diminished velocity profile along the y -direction. Analogous to the impact of a magnetic field, the Hall current effect introduces resistance, subsequently augmenting the thermal performance of the fluid flow. As a consequence, there is an observable rise in the temperature field. The profiles of $g(\eta)$

and $\theta(\eta)$ exhibit elevated levels in the $Fe_3O_4 - Al_2O_3/H_2O$ hybrid nanofluid compared to the $Al_2O_3 - H_2O$ nanofluid and base fluid H_2O , as per observations.

The temperature profile of three fluids exhibit a dual nature influenced by the radiation parameter (Rd), as depicted in Fig. 14. For $0 < \eta < 1$, a decreasing trend in temperature is observed, while it increases for $\eta > 1$. Generally, radiation, deriving energy from liquid particles, serves as a method for heat transfer, generating heat energy in fluid motion and elevating temperature. In Fig. 15, the impact of the Eckert number (Ec) on $\theta(\eta)$ is illustrated, where an increase in Ec results in elevated fluid temperature. This phenomenon is ascribed to the conversion of kinetic energy into internal energy, intensifying temperature distribution across the entire fluid region. The influence of the temperature ratio parameter (θ_w) on $\theta(\eta)$ is portrayed in Fig. 16. The diagram demonstrates that as θ_w increases, both the temperature and the corresponding thermal boundary layer thickness experience augmentation. This occurrence is attributed to the fluid temperature rising significantly above the ambient temperature for elevated θ_w values, leading to an elevation in the overall thermal condition of the fluid. Clearly, based on all the three figures, the temperature profile of $Fe_3O_4 - Al_2O_3/H_2O$ hybrid nanofluid surpasses that of $Al_2O_3 - H_2O$ nanofluid and base fluid H_2O . Figs. 17 depict the influence of the Schmidt digit (Sc) on the concentration profile of three fluids. The Schmidt numeral, representing the relationship between speed and mass diffusivity, induces a reduction in diffusivity, subsequently causing a decrease in fluid concentration as Sc increases.

The Table 5 showcasing the impact of skin friction coefficient in both the x and y directions, as well as the local Nusselt number and Sherwood number, concerning the leading non-dimensional parameters Nt , Nb , M , Rd and λ in this study. An increase in both M and λ results in a noticeable reduction in skin friction along both the x and y axes, whereas variations in the parameters Nt , Nb and Rd show no observable impact on skin friction. The local Nusselt number exhibits a downward trend with increasing values of Nt , Nb , M and λ , whereas a contrasting pattern is evident for Rd , which shows an increase, as these parameters rise. Further, the Sherwood number tends to rise as Nb , M , Rd and λ increase, conversely, it tends to decline as Nt increases.

5. Conclusion

The outcomes of this investigation entail the subsequent conclusions:

- **Thermophoresis Impact:** Increasing thermophoresis parameter (Nt) raises temperature and concentration, but reduces Nusselt and Sherwood numbers.
- **Brownian Motion Effect:** Higher Brownian motion (Nb) increases temperature, decreases concentration, reduces Nusselt number, and increases Sherwood number.

Table 5

The impacts of $\sqrt{Re} C_{fx}$, $\sqrt{Re} C_{fy}$, $Re^{-\frac{1}{2}} Nu_x$ and $Re^{-\frac{1}{2}} Sh_x$ on the $Fe_3O_4 - Al_2O_3/H_2O$ hybrid Nanofluid.

Nt	Nb	M	Rd	λ	$\sqrt{Re} C_{fx}$	$\sqrt{Re} C_{fy}$	$Re^{-\frac{1}{2}} Nu_x$	$Re^{-\frac{1}{2}} Sh_x$
0.1					-2.337435	-1.474208	1.307274	0.640240
0.2					-2.337435	-1.474208	1.307273	0.540703
0.3					-2.337435	-1.474208	1.307272	0.441166
	5				-2.337435	-1.474208	1.307272	0.690009
	10				-2.337435	-1.474208	1.307271	0.714893
	15				-2.337435	-1.474208	1.307269	0.723188
		1			-2.438539	-1.535690	0.480652	0.842306
		1.1			-2.458267	-1.547693	0.321734	0.965652
		1.2			-2.477843	-1.559606	0.164632	1.087649
			0.5		-2.337435	-1.474208	1.307274	0.242091
			1.0		-2.337435	-1.474208	1.442515	0.401867
			1.5		-2.337435	-1.474208	1.552215	0.503883
				0.5	-2.040109	-0.962424	1.407713	0.157392
				1.0	-2.337506	-1.474241	1.304333	0.204008
				1.5	-2.613530	-1.873264	1.200078	0.261482

- **Magnetic Parameter Influence:** As the magnetic parameter (M) rises, the velocity along the x -axis decreases, the y -axis velocity and temperature increase, with lower skin friction and Nusselt numbers, but a higher Sherwood number.
- **Rotation Parameter Outcome:** Higher rotation parameter (λ) decreases velocity profiles, lowers skin friction and Nusselt numbers, and increases the Sherwood number.
- **Hall Current and Radiation:** Increasing the Hall parameter (m) reduces y -axis velocity but increases temperature, while radiation parameter (R_d) shows dual temperature behavior across the fluid layers.
- The Fe_3O_4 - Al_2O_3 / H_2O hybrid nanofluid demonstrates superior thermal performance relative to the nanofluid and base fluid, especially under varying physical parameters.

Hybrid nanofluids such as $Fe_3O_4 - Al_2O_3/H_2O$ offer even broader prospects, notably in augmenting heat transfer, biomedical uses, cooling systems, and environmental remediation. These hybrid nanofluids not only diminish frictional resistance and drag but also serve in lubrication, hydraulic systems and cooling electronic devices. Furthermore, their utility extends to wastewater treatment, flow sensing, diagnostic imaging and purification procedures, illustrating their potential to transform fluid dynamics across multiple domains.

Nanofluids, particularly those comprising $Al_2O_3 - H_2O$, are gaining increasing recognition for their capacity to improve heat transfer efficiency in diverse applications, while remaining both economical and safe. Their adaptability spans from enhancing the cooling of high-temperature electronic components to engine cooling, insulation, drug delivery, and water purification.

Declaration of competing interest

It is declared that we have no conflict of interest.

Data availability

Data will be made available on request.

References

- Choi SUS, Eastman JA. Enhancing thermal conductivity of fluids with nanoparticles. *ASME Int Mech Eng Congress Expo*. 1995;66:99–105.
- Shiva Rao, P. Deka, A numerical analysis on MHD hybrid nanofluid flow and heat transfer over a permeable stretching sheet under the influence of thermal radiation, 2022. DOI:10.21203/rs.3.rs-2185433/v1.
- Sudarsana Reddy P, Sreedevi P, Chamkha AJ. Hybrid nanofluid heat and mass transfer characteristics over a stretching/shrinking sheet with slip effects. *J Nanofluids*. 2023;12:251–260. <https://doi.org/10.1166/jon.2023.1996>.
- Hsiao Kai-Long. To promote radiation electrical MHD activation energy thermal extrusion manufacturing system efficiency by using Carreau-Nanofluid with parameters control method. *Energy*. 2017;130:486–499. <https://doi.org/10.1016/j.energy.2017.05.004>.
- Shankar Goud B, Dharmiaiah G, Hendy Ahmed S, Ali Mohamed R. Flow over a stretchable cylinder with nonlinear heat sources/sinks: magnetic dipoles application. *Case Stud Therm Eng*. 2024;54, 104038. <https://doi.org/10.1016/j.csite.2024.104038>.
- Zainal NA, Nazar R, Naganthran KK, Pop I. MHD flow and heat transfer of hybrid nanofluid over a permeable moving surface in the presence of thermal radiation. *Int J Numer Methods Heat Fluid Flow*. 2021;31(3):858–879. <https://doi.org/10.1108/HFF-03-2020-0126>.
- Khan MN, Ahammad NA, Ahmad S, et al. Thermophysical features of Ellis hybrid nanofluid flow with surface-catalyzed reaction and irreversibility analysis subjected to porous cylindrical surface. *Front Phys*. 2022;10, 986501. <https://doi.org/10.3389/fphy.2022.986501>.
- Pal D, Roy N, Vajravelu K. Thermophoresis and Brownian motion effects on magneto-convective heat transfer of viscoelastic nanofluid over a stretching sheet with nonlinear thermal radiation. *Int J Ambient Energy*. 2022;43(1):413–424. <https://doi.org/10.1080/01430750.2019.1636864>.
- Dharmiaiah G, Goud BS, Shah NA, Faisal M. Numerical analysis of heat and mass transfer with viscous dissipation, Joule dissipation, and activation energy. *Int J Ambient Energy*. 2023;44(1):2090–2102. <https://doi.org/10.1080/01430750.2023.2224335>.
- Hsiao Kai-Long. Combined electrical MHD heat transfer thermal extrusion system using Maxwell fluid with radiative and viscous dissipation effects. *Appl Therm Eng*. 2017;112:1281–1288. <https://doi.org/10.1016/j.applthermaleng.2016.08.208>.
- Hsiao Kai-Long. Micropolar nanofluid flow with MHD and viscous dissipation effects towards a stretching sheet with multimedia feature. *Int J Heat Mass Transf*. 2017; 112:983–990. <https://doi.org/10.1016/j.jheatmasstransfer.2017.05.042>.
- Shankar Goud B, Dharmiaiah G. Role of Joule heating and activation energy on MHD heat and mass transfer flow in the presence of thermal radiation. *Numer Heat Transf Part B: Fundam*. 2023;84(5):620–641. <https://doi.org/10.1080/10407790.2023.2215917>.
- Hsiao Kai-Long. Stagnation electrical MHD nanofluid mixed convection with slip boundary on a stretching sheet. *Appl Therm Eng*. 2016;98:850–861. <https://doi.org/10.1016/j.applthermaleng.2015.12.138.W>.
- Iskandar KBHamzah, Khashi'ie NS, Zainal NA, Kasim ARM, Ishak A, Pop I. Brownian and thermophoresis diffusion effects on magnetohydrodynamic Reiner–Philippoff nanofluid flow past a shrinking sheet. *Alex Eng J*. 2023;67:183–192. <https://doi.org/10.1016/j.aej.2022.12.056>.
- Arshad M, Alharbi FM, Hassan A. Effect of inclined magnetic field on radiative heat and mass transfer in chemically reactive hybrid nanofluid flow due to dual stretching. *Sci Rep*. 2023;13:7828. <https://doi.org/10.1038/s41598-023-34871-9>.
- Abdelmalek Z, Hussain A, Bilal S, Sherif ESM, Thounthong P. Brownian motion and thermophoretic diffusion influence on thermophysical aspects of electrically conducting viscoelastic nanofluid flow over a stretched surface. *J Mater Res Technol*. 2020;9(5):11948–11957. <https://doi.org/10.1016/j.jmrt.2020.08.014>.
- Jagadish VT, Guled CN, Noeiaghdam S, Fernandez-Gamiz U, Govindan V, Balamuralitharan S. Effects of thermophoresis and Brownian motion for thermal and chemically reacting Casson nanofluid flow over a linearly stretching sheet. *Results Eng*. 2022;15, 100448. <https://doi.org/10.1016/j.rineng.2022.100448>.
- Mehta R, Kataria HR. Brownian motion and thermophoresis effects on MHD flow of viscoelastic fluid over stretching/shrinking sheet in the presence of thermal radiation and chemical reaction. *Heat Transfer*. 2021;1–22. <https://doi.org/10.1002/hjt.22307>.
- Carlier MF, Hill TL, Chen Y. Interference of GTP hydrolysis in the mechanism of microtubule assembly: an experimental study. *Proc Natl Acad Sci*. 1984;81(3): 771–775. <https://doi.org/10.1073/pnas.81.3.771>. PMID: 6583675.
- Gangadhar G, Sharath Babu K, Srinivasa Kumar V. Numerical study of hall current effect on MHD nanofluid with inclined plates in the presence of brownian motion and thermophoresis. *Math Stat Eng Appl*. 2023;71(4):8261–8283. <https://doi.org/10.17762/msea.v71i4.1455>.
- Elattar S, Helmi MM, Elkotb MdA, et al. Computational assessment of hybrid nanofluid flow with the influence of hall current and chemical reaction over a slender stretching surface. *Alex Eng J*. 2022;61(12):10319–10331. <https://doi.org/10.1016/j.aej.2022.03.054>.
- Das K, Giri SS, Kundu PK. Influence of Hall current effect on hybrid nanofluid flow over a slender stretching sheet with zero nanoparticle flux. *Heat Transf*. 2021;50: 7232–7250. <https://doi.org/10.1002/hjt.22226>.
- Raizah Z, Alrabaiah H, Bilal M, et al. Numerical study of non-Darcy hybrid nanofluid flow with the effect of heat source and hall current over a slender extending sheet. *Sci Rep*. 2022;12:16280. <https://doi.org/10.1038/s41598-022-20583-z>.
- Alzahrani AK. Effects of hall current and viscous dissipation on bioconvection transport of nanofluid over a rotating disk with motile microorganisms. *Nanomaterials*. 2022;12:4027. <https://doi.org/10.3390/nano1222402726>.
- Suresh Kumar Y, Hussain S, Raghunath K, et al. Numerical analysis of magnetohydrodynamics Casson nanofluid flow with activation energy, Hall current and thermal radiation. *Sci Rep*. 2023;13:4021. <https://doi.org/10.1038/s41598-023-28379-5>.
- Joule JP. On the production of heat by voltaic electricity. In: *Abstr. Pap. Print. Philos. Trans. R. Soc. London. The Royal Society London*; 1843:280–282.
- Lund LA, Asghar A, Rasool G, Yashkun U. Magnetized casson SA-hybrid nanofluid flow over a permeable moving surface with thermal radiation and Joule heating effect. *Case Stud Therm Eng*. 2023;50, 103510. <https://doi.org/10.1016/j.csite.2023.103510>.
- Shamshuddin MD, Khan SU, Beg OA, Beg TA. Hall current, viscous and Joule heating effects on steady radiative 2-D magneto-power-law polymer dynamics from an exponentially stretching sheet with power-law slip velocity: a numerical study. *Therm Sci Eng Prog*. 2020;20, 100732. <https://doi.org/10.1016/j.tsep.2020.100732>.
- Yashkun U, K.Zaimi Alshak, Pop I, Sidaoui R. Hybrid nanofluid flow through an exponentially stretching/shrinking sheet with mixed convection and Joule heating. *Int J Numer Methods Heat Fluid Flow*. 2021;31(6):1930–1950. <https://doi.org/10.1108/HFF-07-2020-0423>.
- Ramzan M, Shah Z, Kumam P, Khan W, Waththayu W, Kumam B. Bidirectional flow of MHD nanofluid with Hall current and Cattaneo-Christove heat flux toward the stretching surface. *PLoS One*. 2022;17(4), e0264208. <https://doi.org/10.1371/journal.pone.0264208>.
- Madiha KT, Satya Narayana PV. Impacts of Joule heating and dissipation on magnetohydrodynamic ternary-hybrid nanofluid (Al_2O_3 - TiO_2 - SiO_2 / H_2O) flow over an elongated sheet with Darcy–Forchheimer medium. *Proc Inst Mech Eng Part E J Process Mech Eng*. 2023. <https://doi.org/10.1177/09544089231200381>.
- Ullah H, Fiza M, Khan K, Batool S, Ghufuran SM, Al-Mekhlafi SM. Effect of joule heating and thermal radiation of MHD boundary layer oldroyd-B nanofluid flow with heat transfer over a porous stretching sheet by finite element method. *J Nanomater*. 2022. <https://doi.org/10.1155/2022/7373631>. Article ID 7373631.
- Elsaid EM, Alshurafat KS. Impact of hall current and joule heating on a rotating hybrid nanofluid over a stretched plate with nonlinear thermal radiation. *J. Nanofluids*. 2023;12(2):548–556. <https://doi.org/10.1166/jon.2023.1927>.

34. Ramzan Md, Mehmood T, Alotaibi H, Ghazwani HAS, Muhammad T. Comparative study of hybrid and nanofluid flows amidst two rotating disks with thermal stratification: statistical and numerical approaches. *Case Stud Therm Eng.* 2021;28, 101596. <https://doi.org/10.1016/j.csite.2021.101596>.
35. Alharbi KAM, Ramzan M, Shahmir N, et al. Comparative appraisal of mono and hybrid nanofluid flows comprising carbon nanotubes over a three-dimensional surface impacted by Cattaneo–Christov heat flux. *Sci Rep.* 2023;13:7964. <https://doi.org/10.1038/s41598-023-34686-8>.
36. Alharbi KAM, Afsar M, Ramzan M, Shahmir N, Kadry S, Saeed AM. Comparative study of hybrid nanofluid flows over a bidirectional stretched surface with the impact of Hall current and ion slip. *Numer Heat Transf Part A: Appl.* 2023:1–17. <https://doi.org/10.1080/10407782.2023.2229513>.
37. Lu Wenjie, Farooq Umar, Imran Muhammad, Chammam Wathek, El Din MSayed, Akgül Ali. Comparative investigations of Ag/H₂O nanofluid and Ag-CuO/H₂O hybrid nanofluid with Darcy-Forchheimer flow over a curved surface. *Nanotechnol Rev.* 2023;12(1), 20230136. <https://doi.org/10.1515/ntrev-2023-0136>.
38. Gul T, Alharbi SO, Khan I, Khan MS, Alzahrani S. Comparative analysis of the flow of the hybrid nanofluid stagnation point on the slippery surface by the CVFEM approach. *Alex Eng J.* 2023;76:629–639. <https://doi.org/10.1016/j.aej.2023.06.025>.
39. Elsaid EM, Abdel-wahed MS. MHD mixed convection Ferro Fe₃O₄/Cu-hybrid-nanofluid runs in a vertical channel. *Chin J Phys.* 2022;76:269–282.
40. Elsaid EM, Abdel-wahed MS. Mixed convection hybrid-nanofluid in a vertical channel under the effect of thermal radiative flux. *Case Stud Therm Eng.* 2021;25, 100913.
41. Eldabe NT, Elbashesy EMA, Emam TG, Essam M. Effect of thermal radiation on heat transfer over an unsteady stretching surface in a micropolar fluid with variable heat flux. *Int J Heat Technol.* 2012;30:93–98.
42. Elsaid EM, Abedel-Aal EM. Darcy-Forchheimer flow of a nanofluid over a porous plate with thermal radiation and brownian motion. *J Nanofluid.* 2023;12(1):55–64.
43. Daniel YS, Daniel SK. Effects of buoyancy and thermal radiation on MHD flow over a stretching porous sheet using homotopy analysis method. *Alex Eng J.* 2015;54(3): 705–712.
44. Mustafa M, Mushtaq A, Hayat T, Alsaedi A. Rotating Flow of Magnetite-Water Nanofluid over a Stretching Surface Inspired by Non-Linear Thermal Radiation. *PLoS One.* 2016;11(2), e0149304. <https://doi.org/10.1371/journal.pone.0149304>.
45. Abdel-Wahed MS. Rotating ferro-nanofluid over stretching plate under the effect of hall current and joule heating. *J Magn Magn Mater.* 2017;429:287–293. <https://doi.org/10.1016/j.jmmm.2017.01.032>.
46. Alzahrani F, Khan MI. Entropy generation and Joule heating applications for Darcy Forchheimer flow of Ree-Eyring nanofluid due to double rotating disks with artificial neural network. *Alex Eng J.* 2022;61(5):3679–3689.
47. Mishra SR, Sun TC, Rout BC, Khan MI, Alaoui MK, Khan SU. Control of dusty nanofluid due to the interaction on dust particles in a conducting medium: numerical investigation. *Alex Eng J.* 2022;61(4):3341–3349.
48. Raja MAZ, Tabassum R, El-Zahar ER, et al. Intelligent computing through neural networks for entropy generation in MHD third-grade nanofluid under chemical reaction and viscous dissipation. *Waves Random Complex Medium.* 2022:1–25.
49. Khan MI, Usman, Ghaffari A, Khan SU, Chu YM, Qayyum S. Optimized frame work for Reiner–Philippoff nanofluid with improved thermal sources and Cattaneo–Christov modifications: a numerical thermal analysis. *Int J Mod Phys B.* 2021;35(06), 2150083.
50. Xiong PY, Nazeer M, Hussain F, et al. Two-phase flow of couple stress fluid thermally effected slip boundary conditions: numerical analysis with variable liquids properties. *Alex Eng J.* 2022;61(5):3821–3830.